Annals of Biomedical Engineering, Vol. 46, No. 12, December 2018 *(© 2018)* pp. 2112–2122
https://doi.org/10.1007/s10439-018-02109-9

Comparison of 4D Flow MRI and Particle Image Velocimetry Using an *In Vitro* Carotid Bifurcation Model

RAFAEL MEDERO,[1,4,5] CARSON HOFFMAN,[2] and ALEJANDRO ROLDÁN-ALZATE[1,3,4]

[1]Department of Mechanical Engineering, University of Wisconsin-Madison, Madison, WI, USA; [2]Department of Medical Physics, University of Wisconsin-Madison, Madison, WI, USA; [3]Department of Biomedical Engineering, University of Wisconsin-Madison, Madison, WI, USA; [4]Department of Radiology, University of Wisconsin-Madison, Madison, WI, USA; and [5]1415 Engineering Drive, Madison, WI 53706, USA

(Received 16 February 2018; accepted 27 July 2018; published online 15 August 2018)

Associate Editor Ender A. Finol oversaw the review of this article.

Abstract—Four-dimensional (4D) Flow magnetic resonance imaging (MRI) enables the acquisition and assessment of complex hemodynamics *in vivo* from different vascular territories. This study investigated the viability of stereoscopic and tomographic particle image velocimetry (stereo- and tomo-PIV, respectively) as experimental validation techniques for 4D Flow MRI. The experiments were performed using continuous and pulsatile flows through an idealized carotid artery bifurcation model. Transverse and longitudinal planes were extracted from the acquired velocity data sets at different regions of interest and were analyzed with a point-by-point comparison. An overall root-mean-square error (RMSE) was calculated resulting in errors as low as 0.06 and 0.03 m/s when comparing 4D Flow MRI with stereo- and tomo-PIV, respectively. Quantitative agreement between techniques was determined by evaluating the relationship for individual velocity components and their magnitudes. These resulted in correlation coefficients (R^2) of 4D Flow MRI with stereo- and tomo-PIV, as low as 0.76 and 0.73, respectively. The 3D velocity measurements from PIV showed qualitative agreement when compared to 4D Flow MRI, especially with tomo-PIV due to the addition of volumetric velocity measurements. These results suggest that tomo-PIV can be used as a validation technique for 4D Flow MRI, serving as the basis for future validation protocols.

Keywords—4D flow MRI, Experimental validation, Tomographic PIV, Stereoscopic PIV, Hemodynamics.

INTRODUCTION

Four-dimensional (4D) Flow magnetic resonance imaging (MRI) is a non-invasive technique used for quantitative and qualitative hemodynamic analysis of blood vessels. 4D Flow MRI can capture time-resolved, three-dimensional velocity vector fields within an area of interest.[20,25,39] Previous application of 4D Flow MRI into the realm of cardiovascular diseases such as, congenital heart disease,[19,27] cerebral aneurysm,[10,22,28] and portal hypertension,[26,32] has shown the potential of this technique to directly impact treatment planning. Limitations of 4D Flow MRI are still present: insufficient spatial resolution for accurate assessment of small vessels and slow velocities near the vessel wall, long scan times and high sensitivity to velocity encoding (VENC) settings.[17,31] The VENC is selected prior to performing the MRI to match the highest predicted velocity value in the area of interest and poor selection can result in low signal-to-noise ratio or velocity aliasing. Therefore, analysis of areas where high and low velocities are both present, such as in aortic dissections and the hepatic circulation, is difficult.

To keep expanding the clinical use of 4D Flow MRI, reliable validation is needed to further improve the accuracy and precision in areas where high and low velocities are present. Previously, velocity and flow measurements from 4D Flow MRI have been validated *in vivo* with 2D phase contrast magnetic resonance (PC-MR),[4,18,30,35] perivascular[8] and Doppler ultrasound,[21,33] on both humans and animals. However, these techniques are limited by their ability to capture small hemodynamic changes over an entire 3D volume and the possibility for confounding factors. Although these experimental studies provided valuable hemodynamic information, the complex flow phenomena present in physiological and pathological conditions demand the need for a validation technique with high spatial and temporal resolution in a controlled setting. *In vitro* systems offer the possibility of making direct,

Address correspondence to Rafael Medero, 1415 Engineering Drive, Madison, WI 53706, USA. Electronic mail: medero2@wisc.edu

controlled measurements, while removing patient and user specific variations.

Particle image velocimetry (PIV), an experimental technique that optically measures flow velocities based on particle displacement, has been commonly used for flow visualization and quantification in numerous engineering applications.[5,6] Recently, PIV has been applied to biomedical applications to capture physiological and pathological flows in multiple cardiovascular areas such as heart valves, aneurysms and vascular stenosis.[3,9,11,13,16] PIV can assess complex velocities in entire flow fields with up to 4 Mpixel resolution and hundreds of frames per second. There are currently three PIV techniques that are appropriate for comparative velocity measurements: 2D PIV, stereoscopic PIV (stereo-PIV) and tomographic PIV (tomo-PIV). 2D PIV resolves 2D velocity components on one single plane and has shown similar results to 4D Flow MRI.[14,34] As MRI's ability to encode velocities in 3D volumes increases, validation techniques with similar dimensionality are needed to best characterize complex flow patterns. Stereo-PIV provides three velocity components along a 2D plane[24] and Tomo-PIV, a recently developed technique, acquires instantaneous measurements of all three velocity components over a 3-dimensional volume.[7] Both stereo- and tomo-PIV provide a promising *in vitro* validation technique for velocity fields gathered from 4D Flow MRI and to our knowledge, no previous results have been reported. Hence, the purpose of this study was to compare 4D Flow MRI with *in vitro* PIV velocity measurements using two different techniques: stereoscopic and tomographic PIV. This effort will provide a basis for the use of stereo- and tomo-PIV in the advancement and validation of 4D Flow MRI.

MATERIALS AND METHODS

Experimental Setup

A silicone model of the carotid artery bifurcation (model: CNB-STWV, Shelley Medical Imaging Technologies, Ontario, CA) (Fig. 1d), composed of the common, internal and external carotid arteries (CCA, ICA and ECA, respectively), was used for *in vitro* PIV and MRI experiments. The vessel inner diameters were: CCA = 8.00 mm, ICA = 5.52 mm and ECA = 4.62 mm. Two sets of experiments were performed, where the first used continuous flow conditions and the second protocol incorporated pulsatile flow.

Continuous Flow

The silicone carotid model was connected to a perfusion pump (Stockert S3, Stockert GmbH, Freiburg, Germany) (Fig. 1a) using medical plastic tubing. The model was placed on the MRI scanner while the pump system was set up in the control room (Fig. 1c); tubing with diameter of 9.525 mm and length of 7.62 m was directed through a perforation on the dividing wall, avoiding any drastic curvatures or kinks that might affect the flow. An inlet flow rate of 1 L/min was ensured at the entrance of the model, resulting in a Reynolds number (Re) of 297. Direct measurement of the inlet flow rate was performed using a non-intrusive ultrasonic flow sensor (Transonic, Ithaca, NY) to verify and ensure an inlet flow rate of 1 L/min during data acquisition. This experimental setup was replicated in the PIV experiments, keeping the tubing length and the height of the model relative to the pump constant.

The circulating fluid was a solution of 42% water and 58% glycerol to match the refractive index of the silicone model (n = 1.41) while keeping a density of 1.14 g/cm^3 and a dynamic viscosity of 0.01017 Pa·s at room temperature. Index matching is required for the PIV techniques to achieve optical transparency, minimizing errors due to the optical distortions of the model and the liquid interface. The fluid was seeded with polyamide particles with mean diameter and density of 20 μm and 1.2 g/cm^3, respectively. These parameters result in a Stokes number lower than 10^{-4}, which ensures that the particles do not interfere with the fluid flow streamlines. The same solution with particles was used for both the MRI and PIV experiments, in order to ensure that the particles were not a confounding factor in the comparison between methods.

Pulsatile Flow

The silicone model was connected to a positive displacement pulsatile pump (model: PD-1100, BDC Laboratories, Wheat Ridge, CO) in line with a hemodynamic conditioning head (Fig. 1b) to control the pressure pulse and produce a nearly physiologic pulse wave. The same control room, MRI scanner, fluid solution, and setup were used as with the continuous flow experiments. Hard PVC tubing of 0.75 in (19.05 mm) diameter, 0.125 in (3.175 mm) thickness and 25 ft (7.62 m) length was used. The pump was set to supply a mean flow rate of 0.75 L/min with a maximum of 1 L/min at a frequency of 60 beats per minute.

4D Flow MRI

MRI scanning was completed on a clinical 3T scanner (Discovery MR 750, GE Healthcare, Waukesha, WI) using a wrist coil. 4D Flow MRI was performed with a 5-pt phase contrast vastly undersampled

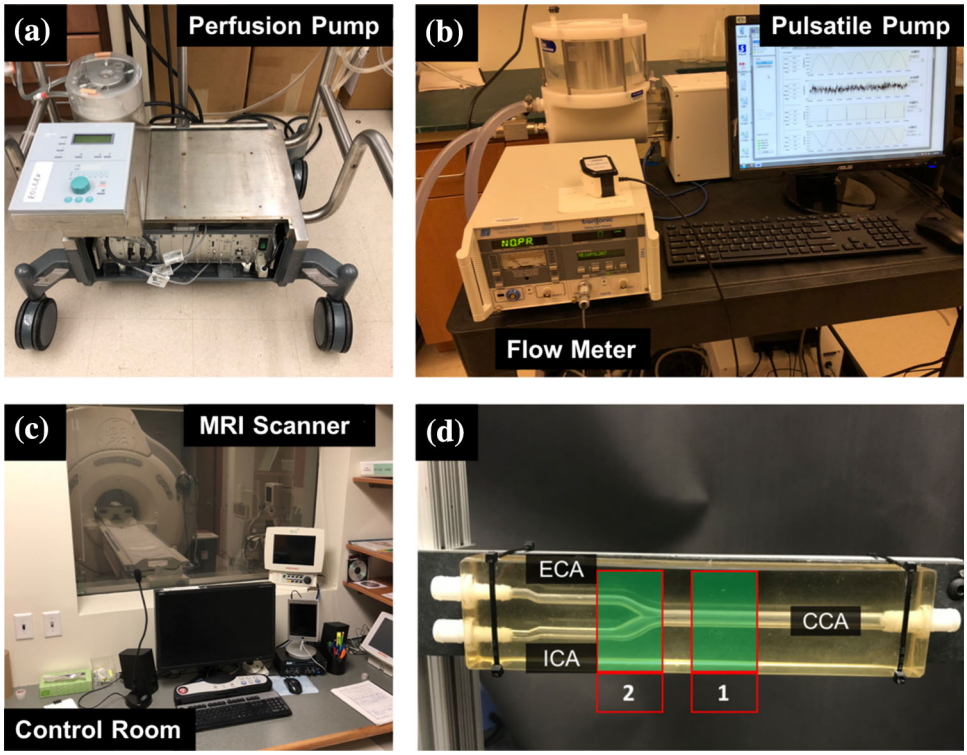

FIGURE 1. (a) Perfusion pump for continuous flow experiments. (b) Pulsatile pump, including the conditioning head on the top left. (c) Control room for the 4D Flow MRI experiments. The room where the scanner is located can be seen through the window. Long tubing was directed through the dividing wall, connecting the pump to the silicone model on the MRI scanner. (d) Silicone *in vitro* model of the carotid artery bifurcation. Data were acquired at the [1] CCA and [2] bifurcation for comparison between velocity measurement techniques.

isotropic projection (PC-VIPR) technique, allowing high spatial and temporal resolution.[12] Imaging parameters were: FOV = 22 × 22 × 22 cm; 0.625 mm acquired isotropic spatial resolution; echo time (TE) = 1.6 ms; repetition time (TR) = 6.4 ms; temporal resolution = 64 ms; scanned time approximately 10 min; and velocity encoding (VENC) = 75 cm/s to account for expected peak velocities of approximately 75 cm/s and to avoid velocity aliasing. MRI was performed while the solution of water and glycerol circulated through the model. Time averaged reconstruction was used[15] for continuous flow experiments. Cardiac gating was used for the pulsatile flow experiments to synchronize the data acquisition to the pulse of the pump. Time resolved reconstruction of the pulsatile 4D Flow MRI dataset was performed retrospectively using the cardiac gating data.

PIV Measurement

Camera Calibration

A 3D calibration plate with two levels was used, which has a defined separation in depth of 1 mm. This plate was placed at the location of the laser sheet while having the same optical distortion as the model to minimize error. The camera calibration was performed on a custom-built silicone casing, shown in Fig. 2a, resulting in the same refractive index as in the experiments. In addition, the calibration plate was submerged in the working fluid to better replicate the optical conditions of the fluid model. The cameras were focused until a clear image of the calibration points on the plate was achieved. Once the cameras were calibrated, the experiments were performed placing the carotid artery bifurcation model at the same distance between the cameras and the laser sheet.

Stereoscopic PIV

All PIV experiments were performed using a Flowmaster PIV system (LaVision, Göttingen, Germany) having a dual-pulse 527 nm Nd:YLF laser (Photonics Industries International, Inc., Long Island, NY), with pulse energy of 40 mJ at 1 kHz. For the stereo-PIV experiments, the laser beam was projected in a direction perpendicular to two high-speed cameras (Phantom v341, Vision Research, Wayne, NJ), which were equipped with 60 mm f/2.8D lenses (Nikon Inc., Melville, NY), as shown in Fig. 2b. The data was acquired at two locations, shown in Fig. 1d, using a 1 mm thick laser sheet aligned to the center of the

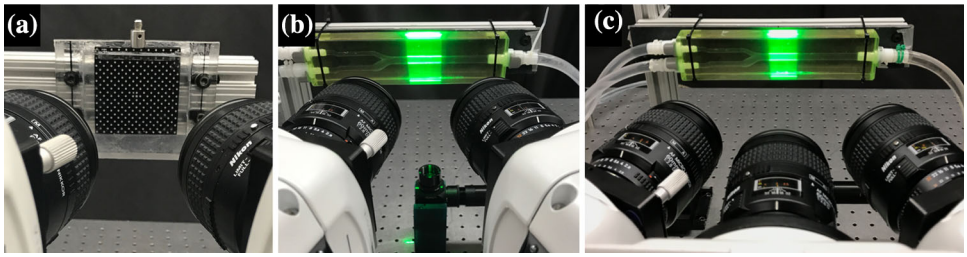

FIGURE 2. (a) Calibration setup used for stereo- and tomo-PIV, showing the black calibration plate within the silicone casing. (b) Stereo PIV and (c) tomo-PIV setups, where the green laser sheet is projected at the longitudinal center of the silicone model.

vessel. Both cameras were mounted on the same side and aligned with an angle of 20° from the focus point. Scheimpflug adapters were used to rotate the image plane with respect to the lens planes, allowing the cameras to focus the image over the entire field of view.

Double-frame images were recorded at a frame rate of 402 Hz, with time separation of 230 μs for a maximum particle displacement of 152 μm. The system acquired 100 sets of images and the experiment was repeated three times for the continuous flow experiments. In the case of pulsatile flow, a total of 400 sets of images, resulting in 1.5 s of acquisition time, were acquired to ensure the inclusion of a complete cardiac cycle (1 s). The images were pre-processed using subtraction of a mean intensity image and Gaussian smoothing (3 × 3) to eliminate errors caused by small differences in refractive index. Moreover, stereo self-calibration was applied to correct errors of misalignment between the calibration plate and the laser sheet by adjusting the coordinate system to the middle of the laser sheet.[36] The resulting images were processed for vector calculation using a multi-pass iteration process with window size of 32 × 32 pixels and 75% overlap for 3 passes. The resulting spatial resolution for stereo-PIV was 0.14 × 0.14 mm. For continuous flow experiments, velocity measurements from the 100 sets of images were averaged to obtain a mean velocity field for each acquisition. For the pulsatile flow experiments, every 20 sets of images were averaged to obtain a total of 20 time steps along the cardiac cycle.

Tomographic PIV

Tomo-PIV was collected using the same experimental setup and recording parameters as for stereo-PIV (Section "Stereoscopic PIV"). To assess repeatability in this newer technique, experiments were performed four times on different days. Figure 2c shows the three-camera configuration with $\theta = \{-25, 0, 25\}$ degrees, obtaining measurement of the three velocity components V_x, V_y, V_z in a volume, which is comprised of a 3 mm thick laser sheet (Fig. 3). This setup is known to increase the reconstruction accuracy when compared to a two-camera setup by adding information from multiple points of view.[7]

Data processing for tomo-PIV required the reconstruction of a volume from the illuminated particles. First, image pre-processing was done following the same parameters used for stereo-PIV, and later applied volume self-calibration to correct errors of misalignment between the calibration plate and the laser sheet.[37] Then, volume reconstruction was performed with the fast multiplicative algebraic reconstruction technique (MART) algorithm explained by Elsinga *et al.*,[7] using 6 iterations. The volumetric reconstructed vector calculation was completed using a multi-pass iteration process with window size 32 × 32 × 32 voxels and 75% overlap for 3 passes. The resulting spatial resolution for tomo-PIV was 0.14 × 0.14 × 0.14 mm. Similar to stereo-PIV, the resultant data sets were averaged to obtain a mean velocity field for each of the four experiments, for the continuous flow experiments, and 20 time steps were obtained by averaging every 20 image set, for the pulsatile flow experiments.

Data Analysis

PIV and 4D Flow MRI images were visualized and quantified in Ensight (CEI Inc., Apex, NC). In order to appropriately compare the 3D techniques with stereo-PIV, a longitudinal plane (x–y) was extracted from 4D Flow MRI and tomo-PIV data sets at the center of the vessel (at locations 1 and 2, Fig. 2b). Additionally, in order to analyze the vessel cross-sectional velocities (z–y), a 1D array from stereo-PIV was estimated by assuming fully developed laminar flow throughout the CCA. A point-by-point comparison was made between techniques by subtracting velocity measurements from a grid created at each plane, using the PIV techniques as the reference values. Stereo-PIV was used as reference value when compared to tomo-PIV. Relationship in velocity components and magnitudes was evaluated by calculating the root-mean-square error (RMSE), linear regression and correlation coefficient (R^2).

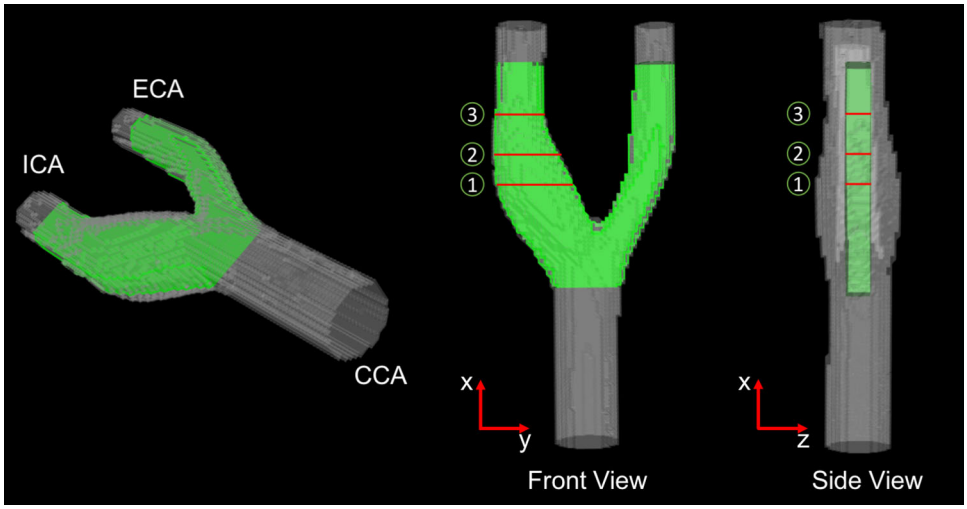

FIGURE 3. Area illuminated by the 3 mm thick laser sheet used for the tomo-PIV analysis at the carotid artery bifurcation model. The red lines represent the cross-sectional planes placed at the ICA for a complex flow analysis. Data were also acquired at the CCA for comparison between techniques.

An estimation of uncertainty was performed to stereo-PIV using the correlation statistics method developed by Wieneke.[38] This method accounts for image disparity, background image noise and out-of-plane particle motion. However, this method has proved to be an accurate estimate of the true error along a plane,[29] not in a volume. Therefore, the experimental uncertainty for tomo-PIV was estimated by calculating the 95% confidence interval for a random sample of points in different planes within the reconstructed volume. To assess the variability between consecutive planes, differences in velocity at the same random points were quantify between two adjacent planes. The variability was found to be lower than 1%, which suggest that the estimated uncertainty made on a plane is representative of a sub-volume of consecutive planes. The average estimated uncertainty was 4.1 and 4.7% for stereo- and tomo-PIV, respectively.

RESULTS

Steady Flow

Tomo- and stereo-PIV were first compared to 4D Flow MRI at the CCA, where the flow can be assumed to be fully developed. For this, a 3 mm transverse plane was extracted from the 4D Flow MRI data, as shown in Fig. 4a, where the green section represents the matched illuminated area by the tomo-PIV laser. Figure 4b shows the 3 mm cross-sectional velocity measured by 4D Flow MRI, tomo-PIV and an estimated plane from stereo-PIV. Error bars represent standard deviations of up to 0.02 and 0.03 m/s for stereo- and tomo-PIV, respectively. Figure 4 includes the percentage difference along the vessel diameter when comparing 4D Flow MRI to PIV. The greatest differences were obtained when Y/Y_{max} was lower than 0.1 and greater than 0.9 (near the walls) for both comparisons. In other areas of the velocity profile, the percentage difference was lower than 10%. The overall RMSE was calculated for each comparison of 4D Flow MRI with stereo- and tomo-PIV, which yielded 0.060 and 0.025 m/s, respectively.

Qualitative analysis was performed comparing tomo-PIV and 4D Flow MRI on the cross-sectional, z–y planes where the flow demonstrated the highest level of complexity (Fig. 5). Both techniques show vortices and acceleration at all three locations, in addition to recirculating flow in the x-direction at location 1. Lower velocity measurements were obtained with 4D Flow MRI in the acceleration regions, demonstrated by the negative values in the point-by-point velocity subtraction. Table 1 shows the statistical results of the comparison at each location for the velocity magnitudes and its individual components. This analysis shows the z-component of velocity as the biggest contributor for error. Yet, excellent correlation was obtained for the velocity magnitude at each plane.

Pulsatile Flow

A comparison of stereo-PIV, tomo-PIV and 4D Flow MRI under pulsatile flow conditions was made at longitudinal planes located at the center of the vessel. Figure 6 shows the velocity distribution in the planes for each method at three different time points of the cardiac cycle. The flow rate, averaged over the three techniques, within one cycle in a cross-sectional plane at the CCA is shown in the top graphs. The standard

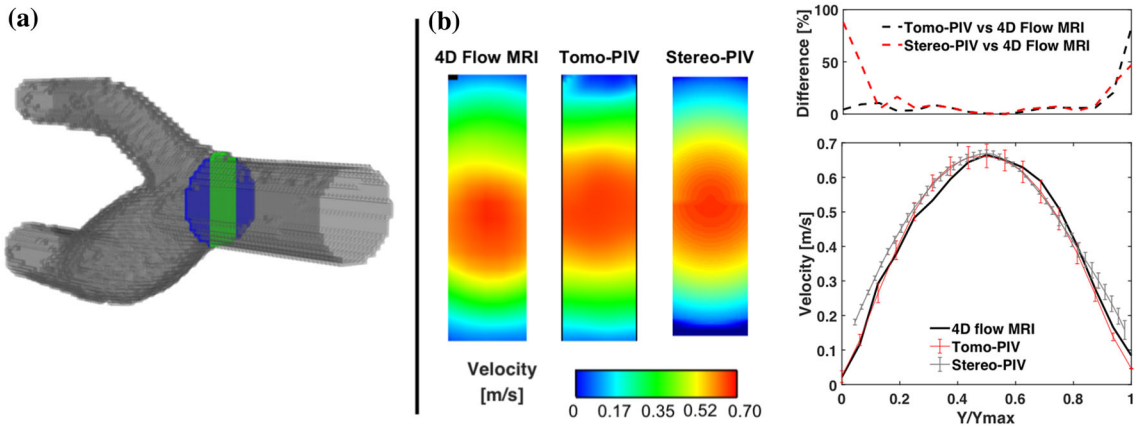

FIGURE 4. (a) Scanned geometry obtained from 4D Flow MRI. The green section shows the 3 mm plane for data quantification. (b) Contour plots at the CCA, showing the velocity distribution measured by 4D Flow MRI, tomo-PIV, and estimated for stereo-PIV in continuous flow experiments. The bottom graph shows the velocity profiles for each technique, where $Y = 0$ is at the top of the plane and Y_{max} at the bottom. Percentage difference along the diameter is shown at the top.

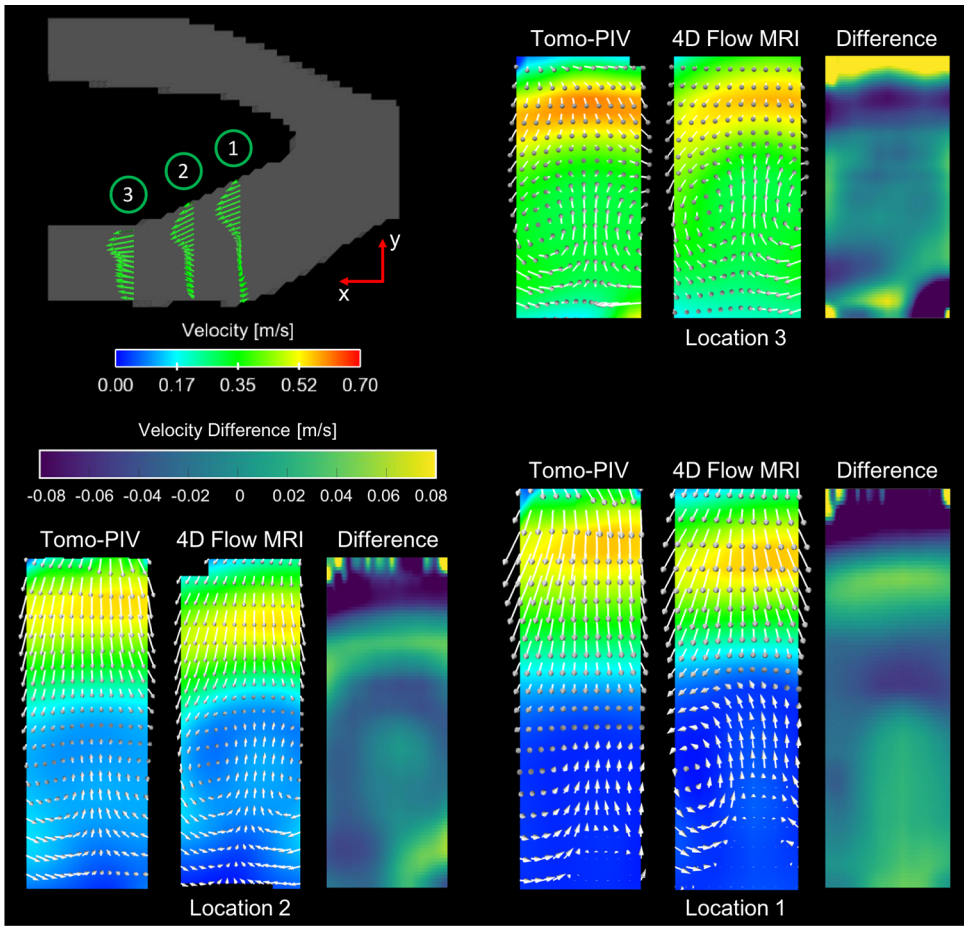

FIGURE 5. Comparison of velocity measurements obtained at three locations on the ICA, as shown at the top left, with constant flow conditions. Directionality of the flow is represented by the velocity vectors superimposed on the contour plots. The velocity difference was calculated by subtracting the velocity magnitudes at each location.

deviation is also included (dotted lines), resulting in 0.02, 0.02 and 0.09 L/min for T1, T2 and T3, respectively. The maximum measured inlet flow was 1.03 L/min, resulting in a 3% error when compared to that specified by the pump. Similar flow behavior was observed with each measuring technique, where recir-

culation and a high velocity region were found on the ICA and ECA, respectively. The spatial velocity comparison between tomo-PIV and 4D Flow MRI

TABLE 1. Relationship evaluation of velocity components (V_x, V_y and V_z) and magnitudes (V_{mag}) between tomo-PIV and 4D flow MRI at the locations shown in Fig. 5.

	RMSE (m/s)	Slope	R^2
Location 1			
V_x	0.032	0.916	0.972
V_y	0.02	1.19	0.959
V_z	0.013	0.645	0.463
V_{mag}	0.044	1.013	0.952
Location 2			
V_x	0.028	0.98	0.965
V_y	0.023	1.036	0.957
V_z	0.019	0.734	0.573
V_{mag}	0.036	1.009	0.956
Location 3			
V_x	0.043	1.214	0.9
V_y	0.031	0.916	0.812
V_z	0.066	1.262	0.426
V_{mag}	0.055	1.099	0.81

The comparison was performed by calculating root-mean-square error (RMSE), slope of the linear regression and correlation coefficient (R^2).

(Fig. 7a) shows the highest differences near the wall, especially in regions with accelerating flow. However, there is high correlation when comparing the complete distribution of velocity magnitudes (Fig. 7b). Table 2 shows the RMSE and the slope of the linear regression for each of the velocity components. There was no correlation for the z-component since the comparison was made on a longitudinal plane and average velocities lower than 0.01 m/s were obtained.

Figure 8 shows velocity profiles at three locations of the same longitudinal plane for time points T1, T2 and T3. Better agreement was found in the CCA at each time step, resulting in an average RMSE of 0.027 and 0.026 m/s for each comparison of 4D Flow MRI with stereo- and tomo-PIV, respectively. On the other hand, instabilities of the flow increased the RMSE to an average of 0.035 and 0.05 m/s at the ICA and ECA, respectively.

DISCUSSION

Controlled *in vitro* experiments are key to evaluate and analyze, with high spatial and temporal resolution, the accuracy and quality of the 4D Flow MRI for a

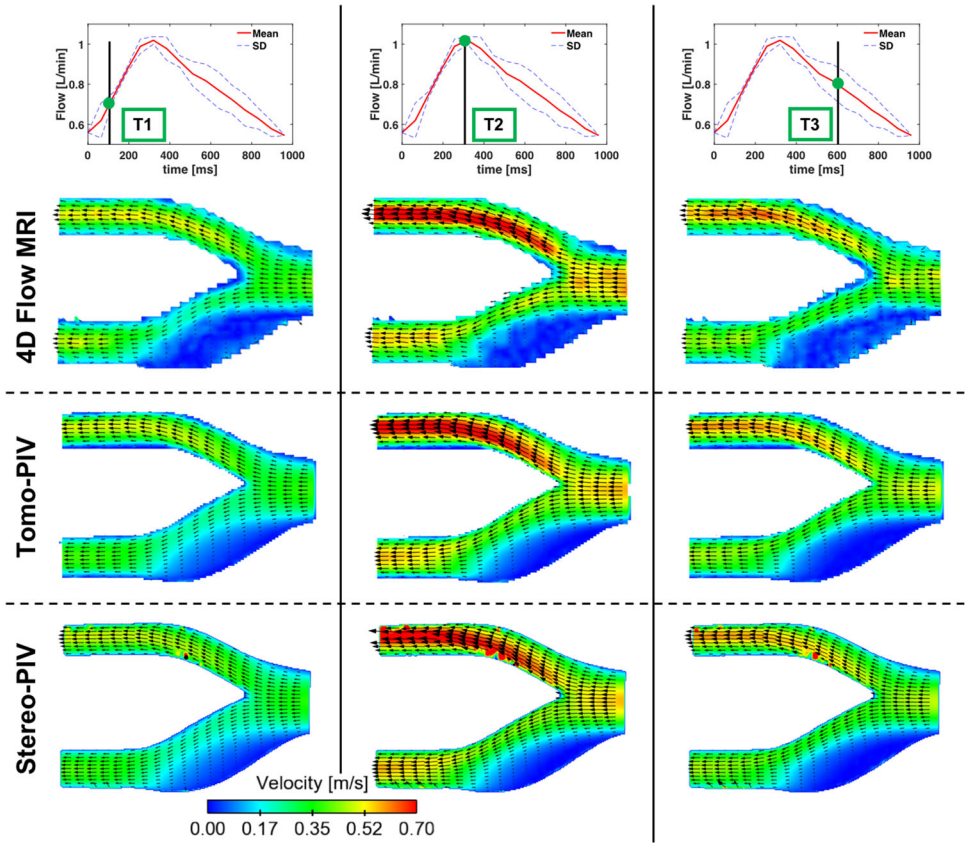

FIGURE 6. Comparison of velocity measurements acquired in the longitudinal plane at the center of the vessel. Directionality of the flow is represented by velocity vectors. Each column shows different time points (T1, T2, and T3) in the sampled cycle. The top graph represents flow rate averaged over techniques and includes the standard deviation (blue dotted lines).

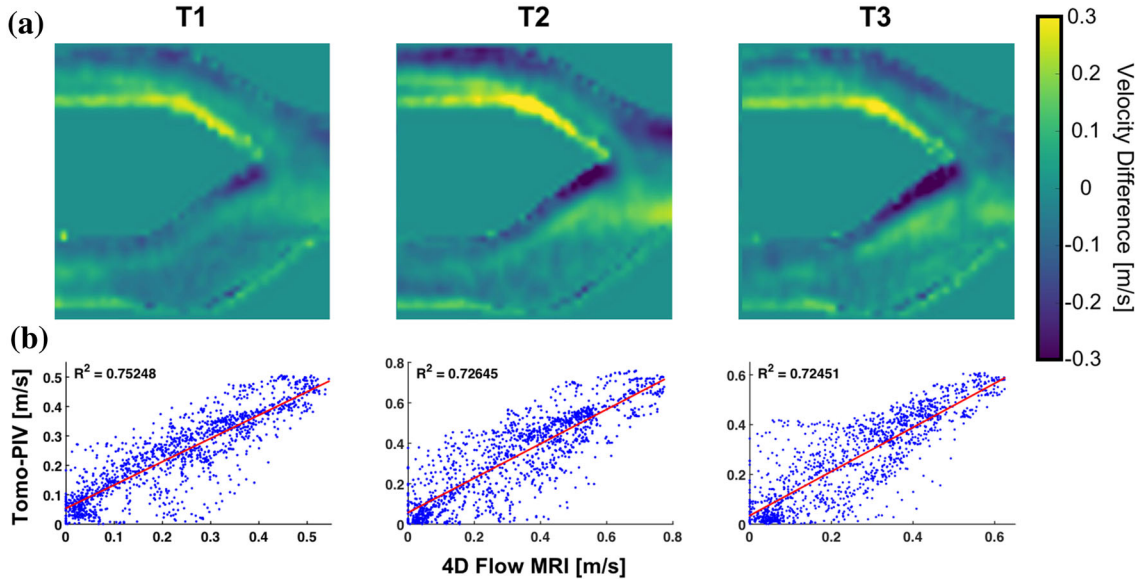

FIGURE 7. (a) Difference in velocity magnitudes obtained for the comparison between 4D Flow MRI and tomo-PIV at the planes shown in Fig. 6. (b) Correlation coefficient (R^2) for the velocity magnitudes obtained at time points T1, T2, and T3. The complete comparison is presented in Table 2.

TABLE 2. Relationship evaluation of velocity components (V_x, V_y and V_z) and magnitudes (V_{mag}) between each technique at the plane shown in Fig. 6.

	RMSE (m/s)			Slope			R^2		
	T1	T2	T3	T1	T2	T3	T1	T2	T3
4D flow MRI vs. tomo-PIV									
V_x	0.066	0.106	0.091	0.773	0.861	0.834	0.767	0.735	0.727
V_y	0.026	0.035	0.036	0.892	0.944	0.808	0.842	0.852	0.763
V_z	0.018	0.018	0.018	0.005	− 0.004	0.02	0	0	0
V_{mag}	0.067	0.108	0.092	0.792	0.85	0.885	0.752	0.726	0.725
4D flow MRI vs. stereo-PIV									
V_x	0.068	0.108	0.09	0.801	0.914	0.856	0.767	0.751	0.744
V_y	0.023	0.03	0.03	0.868	0.919	0.805	0.867	0.881	0.824
V_z	0.04	0.085	0.055	0.048	− 0.114	− 0.085	0	0	0
V_{mag}	0.069	0.112	0.088	0.855	0.948	0.953	0.77	0.755	0.767
Stereo-PIV vs. tomo-PIV									
V_x	0.058	0.09	0.074	0.875	0.857	0.893	0.821	0.81	0.821
V_y	0.016	0.026	0.023	1.013	1.003	0.992	0.942	0.922	0.906
V_z	0.018	0.018	0.018	− 0.001	− 0.002	− 0.003	0	0	0
V_{mag}	0.061	0.098	0.08	0.838	0.806	0.85	0.8	0.777	0.793

The comparison was performed by calculating root-mean-square error (RMSE), slope of the linear regression and correlation coefficient (R^2) for the different time points T1, T2, and T3.

measure of its reliability and thus expand its clinical use. In this study, stereo- and tomo-PIV were used to compare velocity measurements obtained with 4D Flow MRI as an important step in validation protocols. Experiments were performed using continuous and pulsatile flow by means of long tubing (7.62 m) so that the model was in the MRI room while allowing the flow to fully develop, minimizing the inflow effects into the analysis. Results showed high correlation between the techniques at the CCA with both inlet flow conditions. Stereo-PIV demonstrated to be a faster and easier technique to measure a single plane containing a 3D velocity field. Although tomo-PIV takes longer to set up, calibrate and post-process, it provides a volumetric distribution of the flow which allows to study multiple planes within one data set, making it relevant to studies with 4D Flow MRI. Previous work has shown that stereo-PIV can be repeated at multiple

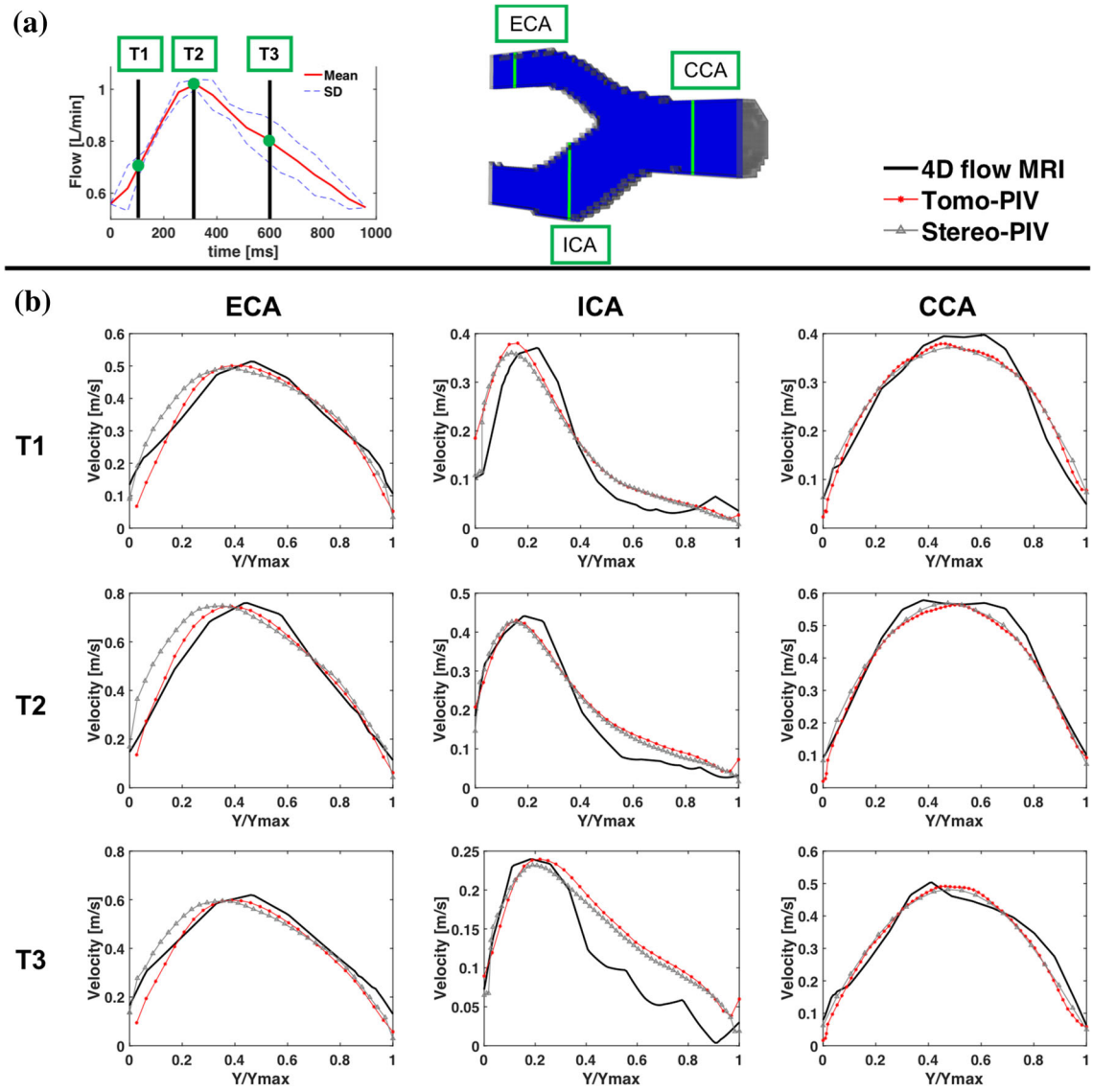

FIGURE 8. (a) Average flow rate with respect to time and definition of discrete measuring time points and plane locations. (b) Comparison of velocity measurements obtained at the locations shown in (a). Rows correspond to time points and columns represent plane or location ($Y = 0$ is at the top of the plane and Y_{max} at the bottom).

spatial locations to then be reconstructed into a 3D volume, and it has been shown that this method agrees well with tomo-PIV.[2]

Stereo-PIV agreed well when compared to the longitudinal planes extracted from tomo-PIV and 4D Flow MRI at the equivalent locations (Figs. 6 and 8). In addition, cross-sectional velocities were estimated at the CCA, where an increase in percentage difference was found near the wall when comparing the velocity profile along a central longitudinal line (Fig. 4), especially when comparing stereo-PIV to 4D Flow MRI. The agreement found in both extracted planes demonstrated the viability of tomo-PIV to measure volumetric velocities while producing multiple planes which closely agree with stereo-PIV acquisitions.

Velocities at the outlet showed a slight difference for 4D Flow MRI when compared to PIV techniques, where the flow becomes unstable, resulting in underestimation of peak velocities. This observation is consistent with other studies and might be due to the fact that the 4D Flow MRI data are averaged over several cycles, whereas PIV is an instantaneous measurement technique.[10,17] This effect was also noted in the vortices shown in Fig. 5, where 4D Flow MRI showed a smoother and clearer pattern than tomo-PIV. Another possible reason for underestimating velocities is the VENC selection, which accurately resolve the slower velocities from noise. Possible solutions are dual VENC approaches or scanning multiple times using different VENC parameters.

However, these are time consuming and not clinically practical at this time.[12,23]

A limitation of the *in vitro* experiments was the lack of plane registration for the spatial comparison. This contributes to the most notable differences in the point-by-point velocity comparisons, especially in Fig. 7, where high differences are seen near the wall. These could be due to misalignments of the planes when being subtracted, since high correlation was obtained when comparing methods with no spatial information. An additional limitation for this comparison is the down-sampling of PIV to match the MRI's. These need to be addressed for validations protocols.

Another limitation of tomo-PIV was the need for a laser thickness of 3 mm to maintain accurate velocity measurements, which did not cover the entire vessel diameter. Increasing the laser thickness to include larger complex models will cause a decrease in the signal to noise ratio and an increase in uncertainty.[1,2] This will be addressed in future studies in addition to a more rigorous assessment of tomo-PIV uncertainty.

In conclusion, this study has shown good quantitative and qualitative agreement between velocity measurements obtained from tomo-PIV and 4D Flow MRI at regions with simple and complex flow behaviors. The consistency in recirculation flow patterns seen in the ICA and the flow acceleration seen in various regions add confidence to the use of 3D PIV methods for validation. The results shown here strongly suggest that tomo-PIV can serve as validation technique for 4D Flow MRI in simplified phantoms with similar Reynolds numbers using continuous or pulsatile flow. Future work will include representations of *in vivo* conditions using patient-specific models and the addition of multiple cardiac cycles to study cycle-to-cycle variations. Thanks to the superior temporal and spatial resolution of PIV, 3D PIV techniques for validation of 4D Flow MRI has multiple clinical applications with the potential to improve understanding of complex flow regimes such as turbulent flow and boundary layer effects in various areas of the body.

ACKNOWLEDGMENTS

The authors are grateful to Dr. Kevin Johnson for his MRI acquisition support at the University of Wisconsin-Madison. Dr. Sylvana García-Rodríguez and Katrina Ruedinger are kindly acknowledged for their critical comments on the manuscript. This study was partially supported by an American Heart Association Scientist Development Grant (#14SDG19690010).

CONFLICT OF INTEREST

The authors state that there are no conflicts of interest related to this research study.

REFERENCES

[1]Bhattacharya, S., J. J. Charonko, and P. P. Vlachos. Stereo-particle image velocimetry uncertainty quantification. *Meas. Sci. Technol.* 28:15301, 2017.

[2]Buchmann, N. A., C. Atkinson, M. C. Jeremy, and J. Soria. Tomographic particle image velocimetry investigation of the flow in a modeled human carotid artery bifurcation. *Exp. Fluids* 50:1131–1151, 2011.

[3]Büsen, M., T. A. S. Kaufmann, M. Neidlin, U. Steinseifer, and S. J. Sonntag. In vitro flow investigations in the aortic arch during cardiopulmonary bypass with stereo-PIV. *J. Biomech.* 48:2005–2011, 2015.

[4]Carlsson, M., J. Töger, M. Kanski, K. M. Bloch, F. Ståhlberg, and E. Heiberg. Quantification and visualization of cardiovascular 4D velocity mapping accelerated with parallel imaging or k-t BLAST: head to head comparison and validation at 1. 5 T and 3 T. *J. Cardiovasc. Magn. Reson.* 13(1):55, 2011.

[5]Day, S. W., and J. C. McDaniel. PIV measurements of flow in a centrifugal blood pump: steady flow. *J. Biomech. Eng.* 127:244–253, 2005.

[6]Elkins, C. J., M. Markl, A. Iyengar, R. Wicker, and J. K. Eaton. Full-field velocity and temperature measurements using magnetic resonance imaging in turbulent complex internal flows. *Int. J. Heat Fluid Flow* 25:702–710, 2004.

[7]Elsinga, G. E., F. Scarano, B. Wieneke, and B. W. Van Oudheusden. Tomographic particle image velocimetry. *Exp. Fluids* 41:933–947, 2006.

[8]Frydrychowicz, A., A. Roldán-Alzate, E. Winslow, D. Consigny, C. A. Campo, U. Motosugi, K. M. Johnson, O. Wieben, and S. B. Reeder. Comparison of radial 4D Flow-MRI with perivascular ultrasound to quantify blood flow in the abdomen and introduction of a porcine model of pre-hepatic portal hypertension. *Eur. Radiol.* 27:5316–5324, 2017.

[9]Gülan, U., B. Lüthi, M. Holzner, A. Liberzon, A. Tsinober, and W. Kinzelbach. Experimental study of aortic flow in the ascending aorta via particle tracking velocimetry. *Exp. Fluids* 53:1469–1485, 2012.

[10]Hope, T. A., M. D. Hope, D. D. Purcell, C. von Morze, D. B. Vigneron, M. T. Alley, and W. P. Dillon. Evaluation of intracranial stenoses and aneurysms with accelerated 4D flow. *Magn. Reson. Imaging* 28:41–46, 2010.

[11]Hopkins, L. M., J. T. Kelly, A. S. Wexler, and A. K. Prasad. Particle image velocimetry measurements in complex geometries. *Exp. Fluids* 29:91–95, 2000.

[12]Johnson, K. M., and M. Markl. Improved SNR in phase contrast velocimetry with five-point balanced flow encoding. *Magn. Reson. Med.* 63:349–355, 2010.

[13]Khodarahmi, I. In vitro validation of flow measurement with phase contrast MRI at 3 tesla using stereoscopic particle image velocimetry and stereoscopic particle image velocimetry. *J. Magn. Reson Imaging* 39(6):1477–1485, 2014.

[14]Kitajima, H. D., K. S. Sundareswaran, T. Z. Teisseyre, G. W. Astary, W. J. Parks, O. Skrinjar, J. N. Oshinski, and A. P. Yoganathan. Comparison of particle image velocimetry

and phase contrast MRI in a patient-specific extracardiac total cavopulmonary connection. *J. Biomech. Eng.* 130:041004, 2008.
[15]Landgraf, B. R., K. M. Johnson, A. Roldán-Alzate, C. J. Francois, O. Wieben, and S. B. Reeder. Effect of temporal resolution on 4D flow MRI in the portal circulation. *J. Magn. Reson. Imaging* 39:819–826, 2014.
[16]Leo, H. L., L. P. Dasi, J. Carberry, H. A. Simon, and A. P. Yoganathan. Fluid dynamic assessment of three polymeric heart valves using particle image velocimetry. *Ann. Biomed. Eng.* 34:936–952, 2006.
[17]Lotz, J., C. Meier, A. Leppert, and M. Galanski. Cardiovascular flow measurement with phase-contrast MR imaging: basic facts and implementation. *RadioGraphics* 22:651–671, 2002.
[18]Markl, M., F. P. Chan, M. T. Alley, K. L. Wedding, M. T. Draney, C. J. Elkins, D. W. Parker, R. Wicker, C. A. Taylor, R. J. Herfkens, and N. J. Pelc. Time-resolved three-dimensional phase-contrast MRI. *J. Magn. Reson. Imaging* 17:499–506, 2003.
[19]Markl, M., J. Geiger, P. J. Kilner, D. Föll, B. Stiller, F. Beyersdorf, R. Arnold, and A. Frydrychowicz. Time-resolved three-dimensional magnetic resonance velocity mapping of cardiovascular flow paths in volunteers and patients with Fontan circulation. *Eur. J. Cardio-thorac. Surg.* 39:206–212, 2011.
[20]Markl, M., A. Harloff, T. A. Bley, M. Zaitsev, B. Jung, E. Weigang, M. Langer, J. Hennig, and A. Frydrychowicz. Time-resolved 3D MR velocity mapping at 3T: improved navigator-gated assessment of vascular anatomy and blood flow. *J. Magn. Reson. Imaging* 25:824–831, 2007.
[21]Meckel, S., L. Leitner, L. H. Bonati, F. Santini, T. Schubert, A. F. Stalder, P. Lyrer, M. Markl, and S. G. Wetzel. Intracranial artery velocity measurement using 4D PC MRI at 3 T: comparison with transcranial ultrasound techniques and 2D PC MRI. *Neuroradiology* 55:389–398, 2013.
[22]Meckel, S., A. F. Stalder, F. Santini, E.-W. Radü, D. A. Rüfenacht, M. Markl, and S. G. Wetzel. In vivo visualization and analysis of 3-D hemodynamics in cerebral aneurysms with flow-sensitized 4-D MR imaging at 3 T. *Neuroradiology* 50:473–484, 2008.
[23]Nett, E. J., K. M. Johnson, A. Frydrychowicz, A. M. Del Rio, E. Schrauben, C. J. Francois, and O. Wieben. Four-dimensional phase contrast MRI with accelerated dual velocity encoding. *J. Magn. Reson. Imaging* 35:1462–1471, 2012.
[24]Prasad, A. K., and R. J. Adrian. Stereoscopic particle image velocimetry applied to liquid flow. *Exp. Fluids* 15:49–60, 1993.
[25]Rebergen, S. A., E. E. Van Der Wall, and J. Doornbos. Magnetic resonance measurement of velocity and flow: technique, validation, and cardiovascular applications. *Am. Heart J.* 126(6):1439–1456, 1993.
[26]Roldán-Alzate, A., A. Frydrychowicz, E. Niespodzany, B. R. Landgraf, K. M. Johnson, O. Wieben, and S. B. Reeder. In vivo validation of 4D flow MRI for assessing the hemodynamics of portal hypertension. *J. Magn. Reson. Imaging* 37:1100–1108, 2013.
[27]Roldán-Alzate, A., S. García-Rodríguez, P. V. Anagnostopoulos, S. Srinivasan, O. Wieben, and C. J. François. Hemodynamic study of TCPC using in vivo and in vitro 4D Flow MRI and numerical simulation. *J. Biomech.* 48:1325–1330, 2015.
[28]Schnell, S., S. A. Ansari, P. Vakil, M. Wasielewski, M. L. Carr, M. C. Hurley, B. R. Bendok, H. Batjer, T. J. Carroll, J. Carr, and M. Markl. Three-dimensional hemodynamics in intracranial aneurysms: influence of size and morphology. *J. Magn. Reson. Imaging* 39:120–131, 2014.
[29]Sciacchitano, A., D. R. Neal, B. L. Smith, S. O. Warner, P. P. Vlachos, B. Wieneke, and F. Scarano. Collaborative framework for PIV uncertainty quantification: comparative assessment of methods. *Meas. Sci. Technol.* 26:74004, 2015.
[30]Stalder, A. F., M. F. Russe, A. Frydrychowicz, J. Bock, J. Hennig, and M. Markl. Quantitative 2D and 3D phase contrast MRI: optimized analysis of blood flow and vessel wall parameters. *Magn. Reson. Med.* 60:1218–1231, 2008.
[31]Stankovic, Z., B. D. Allen, J. Garcia, K. B. Jarvis, and M. Markl. 4D flow imaging with MRI. *Cardiovasc. Diagn. Therapy* 4:173–192, 2014.
[32]Stankovic, Z., Z. Csatari, P. Deibert, W. Euringer, P. Blanke, W. Kreisel, Z. Abdullah Zadeh, F. Kallfass, M. Langer, and M. Markl. Normal and altered three-dimensional portal venous hemodynamics in patients with liver cirrhosis. *Radiology* 262:862–873, 2012.
[33]Stankovic, Z., Z. Csatari, P. Deibert, W. Euringer, B. Jung, W. Kreisel, J. Geiger, M. F. Russe, M. Langer, and M. Markl. A feasibility study to evaluate splanchnic arterial and venous hemodynamics by flow-sensitive 4D MRI compared with Doppler ultrasound in patients with cirrhosis and controls. *Eur. J. Gastroenterol. Hepatol.* 25:669–675, 2013.
[34]Töger, J., S. Bidhult, J. Revstedt, M. Carlsson, and E. Heiberg. Independent validation of four-dimensional flow MR velocities and vortex ring volume using particle imaging velocimetry and planar laser-Induced fluorescence. *Magn. Reson. Med.* 75:1064–1075, 2016.
[35]Wentland, A. L., T. M. Grist, and O. Wieben. Repeatability and INTERNAL CONSISTENCY OF ABDOMINAL 2D and 4D phase contrast MR flow measurements. *Acad. Radiol.* 20:699–704, 2013.
[36]Wieneke, B. Stereo-PIV using self-calibration on particle images. *Exp. Fluids* 39:267–280, 2005.
[37]Wieneke, B. Volume self-calibration for 3D particle image velocimetry. *Exp. Fluids* 45:549–556, 2008.
[38]Wieneke, B. PIV uncertainty quantification from correlation statistics. *Meas. Sci. Technol.* 26:74002, 2015.
[39]Wigstro, L., T. Ebbers, A. Fyrenius, M. Karlsson, J. Engvall, B. Wranne, and A. F. Bolger. Particle trace visualization of intracardiac flow using time-resolved 3D phase contrast MRI. *Magn. Reson. Med.* 41(4):793–799, 1999.